

Probing the muon $g - 2$ with future beam dump experiments

Rupert Coy, Xun-Jie Xu

Service de Physique Théorique, Université Libre de Bruxelles, Boulevard du Triomphe, CP225, 1050 Brussels, Belgium

ABSTRACT: We consider the light Z' explanation of the muon $g - 2$ anomaly. Even if such a Z' has no tree-level coupling to electrons, in general one will be induced at loop-level. We show that future beam dump experiments are powerful enough to place stringent constraints on—or discover—a Z' with loop-suppressed couplings to electrons. Such bounds are avoided only if the Z' has a large interaction with neutrinos, in which case the scenario will be bounded by ongoing neutrino scattering experiments. The complementarity between beam dump and neutrino scattering experiments therefore indicates that there are good prospects of probing a large part of the Z' parameter space in the near future.

Contents

1	Introduction	1
2	Framework	2
2.1	Generic Z' couplings	2
2.2	Kinetic and mass mixing	3
2.3	Muon $g - 2$ and the viable parameter space of muonic Z' models	5
3	Sensitivity of future BD experiments	7
3.1	Influence of neutrino couplings: a simplified scenario	8
3.2	Including hadronic and heavy leptonic states	9
3.3	Case studies for SHiP, SeaQuest, and FASER	11
4	Combined results and discussions	13
5	Conclusions	14

1 Introduction

Following the new measurement of the anomalous magnetic moment of the muon at Fermilab, which has pushed the tension between theory and experiment to 4.2σ [1–3], the $(g-2)_\mu$ anomaly must be considered one of the most compelling indications of new physics.¹ Copious explanations have been proposed in the literature, covering a broad range of possibilities. One notable class of solutions involves extending the Standard Model (SM) gauge sector by an additional $U(1)'$ symmetry, whose gauge boson, Z' , is responsible for the shift in $(g-2)_\mu$ [5]. Not only is this scenario very simple, involving only one extra field, it could potentially be detectable at a large number of different experiments, depending on the mass and couplings of the Z' .

Basic Z' models such as the dark photon, in which the gauge boson couples to SM fermions only via kinetic mixing [6], have been ruled out as a solution to the $(g-2)_\mu$ anomaly. This is due to a combination of collider, beam dump, astrophysical and cosmological bounds, see e.g. [7, 8]. The majority of these bounds are on Z' interactions with electrons, neutrinos and light quarks, while its couplings to second and third generation fermions are relatively less constrained. Consequently, attention has shifted to frameworks of a Z' with flavour-dependent interactions, for instance a gauged $L_\mu - L_\tau$ symmetry wherein the Z' does not couple to electrons or quarks at tree-level [9–11]. These types of models permit the necessary Z' coupling to muons to explain the $(g-2)_\mu$ anomaly while at the same time seemingly avoid many of the most severe experimental constraints, see e.g. [12–16]. The preferred

¹Notwithstanding a lattice calculation which suggests a much smaller discrepancy [4].

parameter space for these scenarios is $m_{Z'} < 2m_\mu$, in which case the Z' cannot decay to muons and so avoids powerful BaBar limits [17].

In reality, the situation is not so straightforward. Even if the Z' does not couple to electrons or quarks at tree level, an effective coupling will be generated at loop level. Despite the loop suppression, there remain a variety of important constraints, which may also depend sensitively on the size of the Z' couplings to neutrinos. In the limit of feeble Z' - ν interactions, there are powerful bounds on Z' -electron couplings down to $\mathcal{O}(10^{-8})$ [8]. Clearly, this is relevant even for loop-induced couplings. This is due in particular to results from historical beam dumps experiments (see e.g. [18]) and forecasts by ongoing and future ones such as NA64 [19], SHiP [20, 21], SeaQuest [22–24], MATHUSULA [25, 26], FASER [27–29], and CODEX-b [30]. These bounds become relatively weaker if the Z' has sizeable interactions with neutrinos. In that case, however, neutrino scattering experiments provide competitive constraints on the Z' [31–36]. There is thus a complementarity between BD and neutrino experiments for probing the Z' solution to the muon $g - 2$ anomaly.

The potentially important role of neutrino couplings in BD experiments and the aforementioned complementarity were largely overlooked in the past, and constitute the main focus of the paper.

This work is organized as follows: in Sec. 2, we establish the conventions for the analysis, including the effects of kinetic mixing, mass mixing and loop diagrams on Z' couplings to fermions. We then outline the present experimental status of the Z' explanation of the $(g - 2)_\mu$ anomaly. The focus turns to future beam dump experiments in Sec. 3. After reviewing the physics of beam dumps, we demonstrate how the bounds depend sensitively on the Z' couplings to both electrons and neutrinos. In Sec. 4, we combine present and expected future bounds, finding that most of the currently viable parameter space will be probed by a combination of future BD and neutrino experiments. Fig. 4.1 summarises our key findings, and we conclude in Sec. 5.

2 Framework

2.1 Generic Z' couplings

We consider a generic framework in which a weakly-coupled, neutral vector boson Z' , typically originating from hidden $U(1)'$ extensions of the SM, is coupled to relevant SM fermions (denoted as f) as follows:

$$\mathcal{L} \supset \sum_f g_f Z'_\mu \bar{f} \gamma^\mu f. \quad (2.1)$$

Here the g_f should be viewed as effective couplings. They may be fundamental, induced by kinetic or mass mixing (see the discussion in the next section), or generated by loop-level processes (see for instance [37]). The SM fermion f can be either chiral (e.g. $f = e_R, \nu_L, u_L$) or non-chiral (e.g. $f = e, \mu, d$). In principle, one could also introduce an axial coupling when considering non-chiral fermions, however in our phenomenological analysis we will assume that the charged leptons couple purely vectorially to the Z' . This provides the most economical solution to the $(g - 2)_\mu$ anomaly and is realised in various popular

scenarios such as $L_\mu - L_\tau$. For neutrinos, since light right-handed neutrinos (ν_R) with sizeable couplings would be in conflict with cosmological observations², we assume that they are either decoupled from the Z' (in which case they can be light), or sufficiently heavy that they do not contribute to the invisible decay width of the Z' . Thus, we take $g_{\nu_\alpha} \equiv g_{\nu_{\alpha L}}$ for neutrino flavour α .

We note here that while in this work we treat the g_f as independent parameters for different fermions, they may potentially be correlated in specific models that address gauge invariance, electroweak symmetry breaking, and kinetic and mass mixing in detail. To remain maximally model-independent, we concentrate on the generic framework proposed in Eq. (2.1). For kinetic and mass mixing, our analysis and results can be readily applied according to the discussion in the next subsection.

2.2 Kinetic and mass mixing

In general, when the SM is extended by an extra $U(1)'$, there is kinetic mixing of the form,

$$\mathcal{L} \supset -\frac{\varepsilon}{2} F^{\mu\nu} F'_{\mu\nu}, \quad (2.2)$$

where $F^{\mu\nu}$ and $F'_{\mu\nu}$ are the field strength tensors of the SM $U(1)_Y$ and $U(1)'$, with ε the kinetic mixing parameter. After electroweak symmetry breaking, there may be mass mixing between the gauge boson of the $U(1)'$ and the Z -boson of the SM, which can be written as³

$$\mathcal{L} \supset \sin\theta m_Z^2 Z^\mu Z'_\mu, \quad (2.3)$$

where θ is the mass mixing parameter. After necessary transformations to redefine the physical mass eigenstates as Z and Z' , Eqs. (2.2) and (2.3) lead to mixing-induced effective couplings of the Z' to all SM fermions, see e.g. Ref. [8, 32]. Here we list the leading-order results for $f = \ell_{L,R}$ ($\ell = e, \mu, \tau$) and ν_L :

$$g_{\ell_L} \approx \varepsilon e \frac{1 - r_m/(2c_W^2)}{1 - r_m} + \frac{1}{2} g_Z (2s_W^2 - 1) \sin\theta, \quad (2.4)$$

$$g_{\ell_R} \approx \varepsilon e \frac{1 - r_m/c_W^2}{1 - r_m} + g_Z s_W^2 \sin\theta, \quad (2.5)$$

$$g_{\nu_L} \approx \varepsilon e \frac{-r_m/(2c_W^2)}{1 - r_m} + \frac{1}{2} g_Z \sin\theta, \quad (2.6)$$

where $(s_W, c_W) \equiv (\sin\theta_W, \cos\theta_W)$ with θ_W the Weinberg angle; $g_Z \equiv g/c_W$ with g the $SU(2)_L$ gauge coupling of the SM, and ε and r_m are defined as

$$\varepsilon \equiv \varepsilon c_W, \quad r_m \equiv \frac{m_{Z'}^2}{m_Z^2}. \quad (2.7)$$

²More specifically, for a sub-GeV Z' coupled to a light ν_R , the effective coupling needs to be smaller than $\sim 10^{-8}$ —see e.g. Fig. 6 in Ref. [38].

³Strictly speaking, since the Z' and Z in Eq. (2.3) are not physical mass eigenstates, one should differentiate the notation in the original basis from that in the mass basis. Here, for simplicity, we neglect the difference. For a rigorous treatment, see Refs. [8, 32].

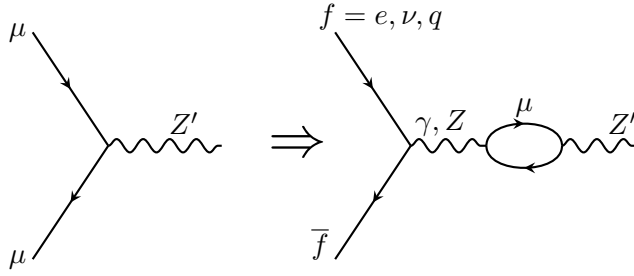


Figure 2.1. The loop diagram from which the presence of the Z' - μ - μ coupling generally implies the existence of Z' couplings to other fermions.

In Eqs. (2.4)-(2.6), the first term comes from kinetic mixing and the second from mass mixing. Note that there are different conventions for the definitions of ε and ϵ in the literature. To avoid potential confusion, we have defined both. Our conventions are consistent with e.g. Refs. [8, 39]. When fermion f has a nonzero $U(1)'$ charge, Q'_f , then one can add $g'Q'_f$ to these effective couplings, where g' is the fundamental $U(1)'$ gauge coupling, as long as both couplings are perturbatively small.

There are some noteworthy limits often considered in the literature⁴:

- The dark photon limit ($r_m \rightarrow 0$): When the Z' is very light, the kinetic mixing leads to photon-like couplings which are parity-conserving for charged fermions and proportional to their electric charges:

$$\lim_{r_m \rightarrow 0, \theta \rightarrow 0} (g_{eL}, g_{eR}, g_{\nu L}) = (\epsilon e, \epsilon e, 0). \quad (2.8)$$

- Hypercharge limit ($r_m \gg 1$): When the Z' is very heavy, one can see that the ϵ terms in Eqs. (2.4)-(2.6) are proportional to their hypercharges while the $\sin \theta$ term vanishes, thus:

$$\lim_{r_m \rightarrow \infty, \theta \rightarrow 0} (g_{eL}, g_{eR}, g_{\nu L}) \propto (1/2, 1, 1/2). \quad (2.9)$$

- Z -like limit ($\epsilon \rightarrow 0$): The $\sin \theta$ terms in Eqs. (2.4)-(2.6) are proportional to the SM Z couplings to the respective fermions. Hence, when Z' is coupled to fermions only via Z' - Z mass mixing, the couplings are Z -like:

$$\lim_{\epsilon \rightarrow \infty} (g_{eL}, g_{eR}, g_{\nu L}) \propto (s_W^2 - 1/2, s_W^2, 1/2). \quad (2.10)$$

It is important to note that while tree-level kinetic and mass mixing could be suppressed by tuning ϵ and θ to sufficiently small values, loop-induced mixing generally exists. Assuming that the Z' interacts with muons (in order to explain the $(g-2)_\mu$ anomaly), this generates couplings of the Z' to electrons and quarks, as illustrated in Fig. 2.1. Unless the tree-level mixing is fine-tuned to cancel the loop-induced mixing⁵, generally we expect

⁴Note that in these limits, all SM fermions are neutral under the $U(1)'$.

⁵This would violate 't Hooft's technical naturalness [40].

an approximate lower bound on g_f by adapting results in Ref. [37] to the loop diagram in Fig. 2.1,

$$|g_f| \gtrsim \frac{\alpha}{3\pi} |g_\mu Q_f| \log \left(\frac{\Lambda^2}{m_\mu^2} \right), \quad (2.11)$$

where Q_f is the electric charge of f , $\alpha \equiv e^2/(4\pi)$, and Λ denotes the new physics scale at which UV divergences are cancelled. In the case of a gauged $L_\mu - L_\tau$, for instance, which is a popular model to address the muon $g - 2$ anomaly, the loop diagram of Fig. 2.1 combined with a similar τ loop is free from UV divergences and leads to the loop-induced couplings [41],

$$g_f = -\frac{\alpha}{3\pi} g_\mu Q_f \log \left(\frac{m_\mu^2}{m_\tau^2} \right). \quad (2.12)$$

As it has been shown in previous studies (see e.g. [8, 33, 42]), the loop-induced couplings play a crucial role in the $L_\mu - L_\tau$ model when confronting it with existing experimental constraints.

2.3 Muon $g - 2$ and the viable parameter space of muonic Z' models

The muonic coupling, g_μ , can be responsible for the discrepancy between the SM prediction and experimental measurements of the muon's anomalous magnetic moment. The contribution of a Z' can be evaluated using the general formula [43],

$$\Delta a_\mu = \frac{g_\mu^2}{4\pi^2} \left(\frac{m_\mu}{m_{Z'}} \right)^2 \int_0^1 \frac{(1-x)x^2}{1-x + (m_\mu/m_{Z'})^2 x^2} dx. \quad (2.13)$$

Here we have assumed that the Z' couples purely vectorially to muons, as mentioned in Sec. 2.1. The recent Fermilab measurement of a_μ combined with the previous BNL E821 result gives [1–3]

$$a_\mu(\text{Exp}) - a_\mu(\text{SM}) = (25.1 \pm 5.9) \times 10^{-10}, \quad (2.14)$$

which indicates a 4.2σ deviation. Using the value in Eq. (2.14), we plot green bands in Fig. 2.2 which gives the region where the Z' reduces the tension to within 1σ . As can be seen, for $m_{Z'} \ll m_\mu$, g_μ needs to be around 4.5×10^{-4} to account for the discrepancy. For $m_{Z'} \gg m_\mu$, however, the required magnitude of g_μ increases approximately linearly with $m_{Z'}$, $g_\mu \approx 0.05 \times (m_{Z'}/10 \text{ GeV})$.

Depending on Z' interactions with other SM fermions, there are various experimental constraints. If the Z' couples exclusively to the muon (though this is theoretically unlikely, especially when taking gauge invariance and loop corrections into consideration), only collider searches for 4μ final states (e.g. $e^+e^- \rightarrow \mu^+\mu^-Z'$ with $Z' \rightarrow \mu^+\mu^-$) can constrain it. BaBar [17] and CMS [44] 4μ searches have excluded the Z' explanation of the anomaly for $m_{Z'} > 2m_\mu$, as shown in the upper left panel of Fig. 2.2.

From the point of view of gauge invariance, given a coupling to μ , the Z' is likely also to have couplings to $\nu_{\mu L}$ with g_{ν_μ} comparable to $g_{\mu L}$.⁶ When the Z' has a neutrino coupling, neutrino scattering data can be used to constrain it. There are various important

⁶It might be possible that Z' only couples to right-handed leptons, so that this argument does not apply.

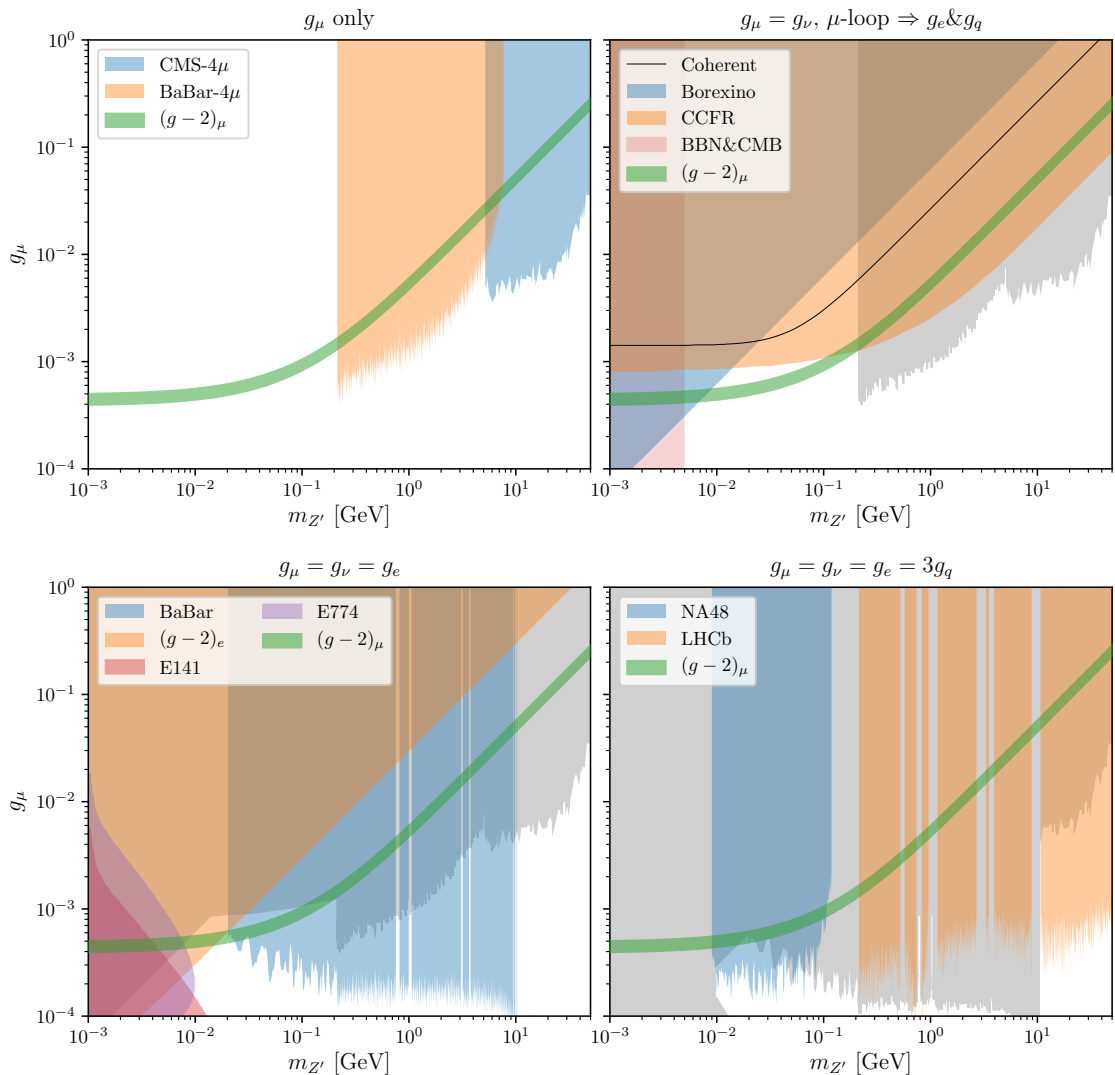


Figure 2.2. Current viable parameter spaces for the Z' when it couples exclusively to μ (upper left), couples equally to μ and $\nu_{\mu,L}$ (upper right), couples universally to leptons (lower left), or couples to all SM fermions (lower right). The green band reduces the muon $g-2$ anomaly to within 1σ . Grey bounds correspond to ones already introduced in previous panels.

bounds, including from $\nu_\mu + e^-$ (Borexino [8, 45]) and $\nu_\mu + N$ (COHERENT [33]) elastic scattering⁷, and $\nu_\mu + N \rightarrow \nu_\mu + N + \mu^+ + \mu^-$ trident scattering (CCFR [12]), shown in the upper right panel under the assumption $g_{\nu_\mu} = g_\mu$. The neutrino elastic scattering bounds are derived from one-loop processes that involve a muon loop which connects Z' to γ , and hence to electrons and nucleons. The trident scattering corresponds to opening the loop, which leads to two muons in the final state.

⁷Another ν_μ elastic scattering experiment, CHARM II, provides the most restrict bound for $m_{Z'} \gtrsim 100$ MeV among ν_μ elastic scattering experiments, but as we have checked, in this regime it is weaker than the CCFR bound—see e.g. [31, 32].

When $m_{Z'}$ is $\mathcal{O}(\text{MeV})$, cosmological constraints from Big Bang Nucleosynthesis (BBN) and Cosmological Microwave Background (CMB) are also relevant. The bounds depend on the Z' coupling to neutrinos and to electrons. Ref. [46] studied the bound on $m_{Z'}$ as a function of the electron to neutrino annihilation ratio. For our purposes, this refers to the ratio of the decay rates into electrons and neutrinos:

$$\frac{\Gamma(Z' \rightarrow e^+e^-)}{\Gamma(Z' \rightarrow \nu^+\nu^-)} \approx \frac{2g_e^2}{g_\nu^2}, \quad (2.15)$$

with the factor of 2 since we sum over final state spins, where we define

$$g_\nu^2 \equiv g_{\nu_e}^2 + g_{\nu_\mu}^2 + g_{\nu_\tau}^2. \quad (2.16)$$

We take the BBN+Planck row of table VI in Ref. [46] and interpolate between the data points to obtain the bounds. Depending on this ratio, it varies from 1.3 to 9.4 MeV. For the upper right panel of Fig. 2.2, using the loop-induced coupling given by Eq. (2.12) for g_e , we find that the bound is $m_{Z'} \gtrsim 4.9$ MeV, although it should be kept in mind that this number has an $\mathcal{O}(1)$ uncertainty. There is also a bound on Z' couplings to neutrinos due to white dwarf cooling [47]. However, since the constraint is very similar to the one obtained from Borexino but relatively more uncertain, it is not included in the plots.

In the lower panels of Fig. 2.2, we impose further constraints assuming the presence of tree-level electron and quark couplings. In this case, collider experiments (e.g. BaBar, NA48, LHCb) are able to search directly for a Z' resonance. Moreover, electron $g-2$ and beam dump (e.g. E774, E141)⁸ experiments provide complementary constraints. These constraints were obtained by employing the DARKCAST package [7].

Fig. 2.2 demonstrates that in order to accommodate the muon $g-2$ anomaly, the Z' boson needs to have suppressed couplings to electrons and light quarks in comparison to g_μ , i.e.

$$|g_\mu| \gtrsim \{|g_e|, |g_\nu|, |g_u|, |g_d|\}. \quad (2.17)$$

From now on, Eq. (2.17) will be considered as a guiding principle when we are concerned with experimental constraints.

3 Sensitivity of future BD experiments

Future beam dump (BD) experiments such as SHiP and SeaQuest have great potential to probe a light, weakly-interacting Z' , provided that its invisible decay width is not too large. In the present framework, where we do not introduce any new fermions, only neutrinos contribute to the invisible decay width. Therefore, the BD sensitivity depends largely on the strength of neutrino couplings, g_ν .

To illustrate the influence of g_ν , we start in Sec. 3.1 with a simplified scenario where only g_e and g_ν are present, and then generalise in Sec. 3.2 to more realistic situations where heavy leptons (μ, τ) and hadronic states are also taken into account. Then in Sec. 3.3 we perform case studies for SHiP, FASER, and SeaQuest.

⁸Other beam dump experiments such as E137 and Orsay are less restrictive in the region of parameter space we consider.

3.1 Influence of neutrino couplings: a simplified scenario

In the presence of only g_e and g_ν couplings, the Z' can be produced at the target in BD experiments via the bremsstrahlung process, $e^- + N \rightarrow e^- + N + Z'$, with the production cross section proportional to g_e^2 ,

$$\sigma_{\text{prod}} \propto g_e^2. \quad (3.1)$$

Once produced, the Z' particle decays during its flight and causes an observable signal only if it penetrates the shielding material (of length L_{sh}) and decays to visible states within the fiducial decay region (of length L_{dec}). The probability of the Z' flying through the shielding and decaying in the fiducial decay region is

$$P = e^{-L_{\text{sh}}/L_{\text{flight}}} \left(1 - e^{-L_{\text{dec}}/L_{\text{flight}}}\right), \quad (3.2)$$

where the mean flight distance, L_{flight} , is given by

$$L_{\text{flight}} = \frac{\tau_0 v}{\sqrt{1 - v^2}}, \quad v = \frac{p_{Z'}}{\sqrt{m_{Z'}^2 + p_{Z'}^2}}. \quad (3.3)$$

Here v , $p_{Z'}$, and τ_0 denote the velocity, momentum, and lifetime (at rest) of the Z' particle, respectively.

Decaying in the fiducial decay region is not enough. To be detectable, the Z' must decay to visible final states (e^+e^- , $\mu^+\mu^-$, or hadronic states). This is taken into account by including the branching ratio of visible decays, BR_{vis} . Thus, the event rate at the detector is given by

$$R \propto \sigma_{\text{prod}} \cdot P \cdot \text{BR}_{\text{vis}}. \quad (3.4)$$

Since in this simplified scenario the Z' only decays to electrons and neutrinos, BR_{vis} and τ_0 are given by

$$\text{BR}_{\text{vis}} = \frac{2g_e^2}{g_\nu^2 + 2g_e^2}, \quad (3.5)$$

$$\tau_0^{-1} = \Gamma_{Z' \rightarrow \nu\bar{\nu}} + \Gamma_{Z' \rightarrow e\bar{e}} \approx \frac{m_{Z'}}{12\pi} \left(\frac{1}{2}g_\nu^2 + g_e^2 \right), \quad (3.6)$$

where we have neglected the electron mass.

Substituting Eqs. (3.5) and (3.6) into Eq. (3.4), we obtain R as a function of g_e , g_ν and $m_{Z'}$. The absolute magnitude of R depends on the exposure time, beam energy and luminosity, target material, etc. To avoid these experiment-dependent details, we make the replacement $\sigma_{\text{prod}} \rightarrow g_e^2$ in Eq. (3.4) and define a dimensionless event rate,

$$\bar{R} \equiv g_e^2 \cdot P \cdot \text{BR}_{\text{vis}}. \quad (3.7)$$

Assembling the above pieces, we obtain

$$\bar{R} = \frac{g_e^4}{g_e^2 + g_\nu^2/2} e^{-\lambda_{\text{sh}}(g_e^2 + g_\nu^2/2)} \left[1 - e^{-\lambda_{\text{dec}}(g_e^2 + g_\nu^2/2)} \right], \quad (3.8)$$

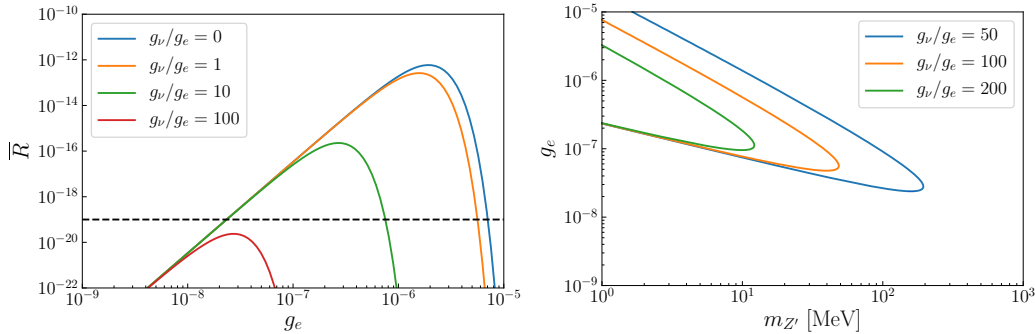


Figure 3.1. Left: the dimensionless event rate \bar{R} (defined in Eq. (3.8)) as a function of g_e and g_ν , fixing $m_{Z'} = 100$ MeV. The black horizontal line represents a hypothetical experimental sensitivity at $\bar{R} = 10^{-19}$ for the purpose of illustration. Right: contours of $\bar{R}(m_{Z'}, g_e) = 10^{-19}$, demonstrating the different hypothetical experimental sensitivities to $m_{Z'}$ and g_e .

where

$$\lambda_{\text{sh/dec}} \equiv L_{\text{sh/dec}} \frac{m_{Z'}^2}{12\pi p}. \quad (3.9)$$

In the left panel of Fig. 3.1, we plot \bar{R} - g_e curves with g_ν/g_e fixed at a few given values. We took $p_{Z'} = 200$ GeV, $L_{\text{sh}} = 60$ m, $L_{\text{dec}} = 50$ m, similar to the specifications for SHiP [20]. For illustration, we plot a black dashed line at $\bar{R} = 10^{-19}$ as a hypothetical experimental sensitivity. Typically, a BD experiment is sensitive to g_e in a certain interval $g_e \in [g_{\text{lower}}, g_{\text{upper}}]$ where g_{lower} and g_{upper} are determined by the intersection of the \bar{R} - g_e curve with the black dashed line.

The shape of these curves can be understood as follows. When g_e is sufficiently small, BD experiments lose sensitivity because (i) the Z' production rate is suppressed, and (ii) the probability of the Z' decaying in the fiducial region is suppressed (τ_0 and L_{flight} are too large, so most decays happen after the Z' has flown further than $L_{\text{sh}} + L_{\text{dec}}$). On the other hand, when g_e is too large the BD experiments also lose sensitivity due to small L_{flight} , in which case most of the particles decay in the shielding. As can be seen from the left panel of Fig. 3.1, the size of g_ν/g_e can significantly affect g_{upper} but has less impact on g_{lower} . As g_ν/g_e increases, g_{upper} decreases because BR_{vis} is reduced. When g_{upper} approaches g_{lower} , the experiment quickly loses sensitivity.

In the right panel of Fig. 3.1, we plot contours of $\bar{R} = 10^{-19}$ in the $m_{Z'}$ - g_e plane. If $\bar{R} = 10^{-19}$ is interpreted as the experimental sensitivity, then the experiment will be able to probe the regions enclosed by these contours. As is shown, when g_ν/g_e increases, these contours shrink not only vertically but also horizontally. This implies that larger invisible decay widths of the Z' will not only lead to smaller intervals of $[g_{\text{lower}}, g_{\text{upper}}]$, but will also reduce the experimental sensitivity to a heavy Z' .

3.2 Including hadronic and heavy leptonic states

The simplified analysis above grasps the main features of BD constraints, such as the existence of g_{lower} and g_{upper} , and the effect of g_ν . In more realistic situations, additional

decay channels (in particular hadronic states) and the dependence of σ_{prod} on $m_{Z'}$ need to be taken into account. We turn to this now.

For $m_{Z'} > 2m_\mu \approx 212$ MeV, the decay mode $Z' \rightarrow \mu\bar{\mu}$ opens up. For even higher masses, the Z' can also decay to hadronic states. Including heavy leptonic final states is straightforward. In the case of $Z' \rightarrow \mu\bar{\mu}$, the partial decay width is given by (see e.g. [39])

$$\Gamma_{Z' \rightarrow \mu\bar{\mu}} = \frac{g_\mu^2}{12\pi} m_{Z'} \sqrt{1 - \frac{4m_\mu^2}{m_{Z'}^2}} \left(1 + \frac{2m_\mu^2}{m_{Z'}^2} \right). \quad (3.10)$$

For Z' masses above about 3.5 GeV, the $Z' \rightarrow \tau\bar{\tau}$ decay mode could also be relevant, and can be included using Eq. (3.10) with $m_\mu \rightarrow m_\tau$ and $g_\mu \rightarrow g_\tau$.

The widths of possible hadronic decay modes ($Z' \rightarrow \text{hadrons}$) can be computed using the hadron-to-muon cross section ratio of e^+e^- collisions,

$$\mathcal{R}(\sqrt{s}) = \frac{\sigma(e^+e^- \rightarrow \gamma^* \rightarrow \text{hadrons})}{\sigma(e^+e^- \rightarrow \gamma^* \rightarrow \mu\bar{\mu})}, \quad (3.11)$$

where \sqrt{s} is the the center-of-mass energy. The \mathcal{R} ratio has been well determined by e^+e^- collision data for $0.3 \text{ GeV} \lesssim \sqrt{s} \lesssim 200 \text{ GeV}$.⁹ Given the experimentally measured \mathcal{R} values, the total hadronic decay width of Z' is given by

$$\Gamma_{Z' \rightarrow \text{had.}} = \left(\frac{g_q}{eQ_q} \right)^2 \Gamma_{\gamma^* \rightarrow \mu\bar{\mu}} \mathcal{R}(m_{Z'}), \quad (3.12)$$

where Q_q is the electric charge of quark q and we have assumed that Z' -quark couplings are photon-like so that g_q/Q_q are independent of the type of quarks. This is the case for the well-studied dark photon scenario, see the dark photon limit in Sec. 2.2. For more general couplings, if hadronic decays are subdominant compared to $Z' \rightarrow \mu\bar{\mu}$, one can still neglect the difference between g_u/Q_u and g_d/Q_d . The virtual photon decay width $\Gamma_{\gamma^* \rightarrow \mu\bar{\mu}}$ can be computed using Eq. (3.10) with $g_\mu^2 \rightarrow e^2$.

In the presence of decays to hadronic ($m_{Z'} > 2m_\pi$) and heavy leptonic ($m_{Z'} > 2m_\mu$) states, the BR_{vis} of Eq. (3.5) is modified to

$$\text{BR}_{\text{vis}} = 1 - \frac{\Gamma_\nu}{\Gamma_\nu + \Gamma_\ell + \Gamma_{\text{had.}}}, \quad (3.13)$$

where Γ_ν , Γ_ℓ , and $\Gamma_{\text{had.}}$ are the decay widths of $Z' \rightarrow \nu\bar{\nu}$, $Z' \rightarrow \ell\bar{\ell}$ ($\ell = e, \mu, \tau$), and $Z' \rightarrow \text{hadrons}$, respectively. The extra decay modes also modifies the lifetime τ_0 in Eq. (3.6) to

$$\tau_0 = (\Gamma_\nu + \Gamma_\ell + \Gamma_{\text{hadrons}})^{-1}. \quad (3.14)$$

It is also important to note that when Z' is heavy, the production cross section becomes dependent on $m_{Z'}$. Therefore, for SHiP-like experiments, we modify Eq. (3.7) as follows,

$$\bar{R} \equiv g_p^2 \cdot \frac{\sigma_{\text{prod}}}{\sigma_{\text{prod}}^*} \cdot P \cdot \text{BR}_{\text{vis}}, \quad (3.15)$$

⁹See Fig. 52.2 of [48] or Fig. 2 of [7]. The data is available from <https://pdg.lbl.gov/2021/hadronic-xsections/>

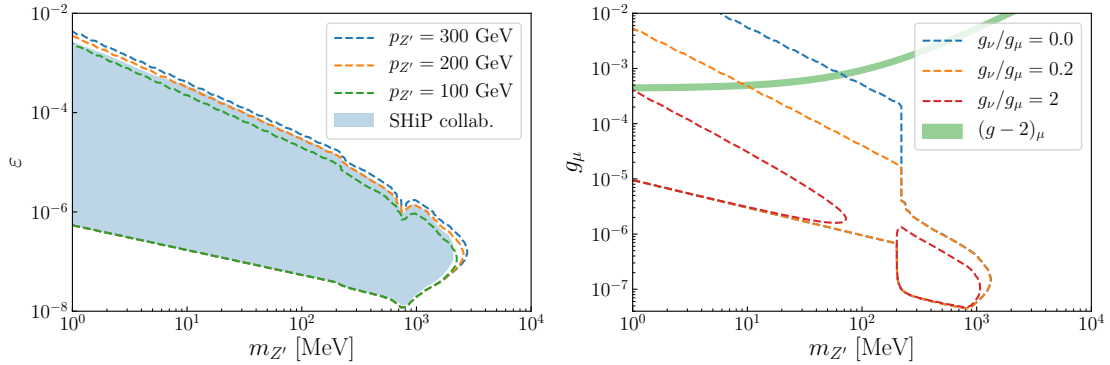


Figure 3.2. Left: Reproduced bounds (dashed) on ε compared to the bound published by the SHiP collaboration [39] (blue shaded). Right: Bounds on the muonic coupling, g_{μ} , due to the invisible decay of Z' . The green band in the right panel is the same as in Fig. 2.2, and couplings of Z' to the electron and quarks are assumed at the loop-induced level given by Eq. (2.12).

where g_p denote the effective coupling of Z' to the proton, σ_{prod} can be obtained from e.g. Fig. 4 in Ref. [39]¹⁰ and $\sigma_{\text{prod}}^* \equiv \sigma_{\text{prod}}(m_{Z'} = 100 \text{ MeV})$.

3.3 Case studies for SHiP, SeaQuest, and FASER

In the left panel of Fig. 3.2, we apply Eq. (3.15) to reproduce the SHiP sensitivity curves for the dark photon scenario with $g_f = \varepsilon c_W e Q_f = \varepsilon e Q_f$. The blue shaded region represents the result published by the SHiP collaboration (taken from the upper panel in Fig. 13 of Ref. [39]) and the dashed curves are produced by extracting contours of $\bar{R}(m_{Z'}, \varepsilon)$, which are fixed at certain values so that the resulting lower bounds at $m_{Z'} = 100 \text{ MeV}$ match the SHiP result ($\varepsilon = 5.28 \times 10^{-8}$). As indicated in the plot, the momentum p is fixed at several values below the proton beam energy (400 GeV). We take $L_{\text{sh}} = 60 \text{ m}$ and $L_{\text{dec}} = 50 \text{ m}$ for the shielding and decay lengths, following Refs. [20, 39]. The specific values of \bar{R} for the three contours (blue, orange, green) to match $\varepsilon = 5.28 \times 10^{-8}$ at $m_{Z'} = 100 \text{ MeV}$ are $(0.5, 0.75, 1.5) \times 10^{-20}$, respectively.

The plot shows that Eq. (3.15) can rather accurately describe the experimental sensitivity in the dark photon scenario. The choice of the specific value of $p_{Z'}$ does not affect the result significantly, as long as it is a significant fraction of the incoming proton energy. This allows us to recast the SHiP bound on the dark photon to give bounds on a Z' with invisible decays.

In the right panel of Fig. 3.2, we set $p_{Z'} = 200 \text{ GeV}$ and $\bar{R} = 0.75 \times 10^{-20}$ (corresponding to the orange curve in the left panel) to generate the SHiP bound on a Z' with $g_{\nu} = (0, 0.2, 2)g_{\mu}$. In addition, we assume g_p and g_e are loop-induced (see Fig. 2.1) using

¹⁰Ref. [39] adopted two approaches to evaluate the production cross section. One included the standard dipole form factor, while the other took into account the possibility of nuclear resonance enhancement, referred to as the vector meson dominance (VMD) model. The former leads to a more conservative result than the later, although the difference becomes significant only for $m_{Z'} \gtrsim 500 \text{ MeV}$. In this work, we adopt the cross section obtained from the former approach.

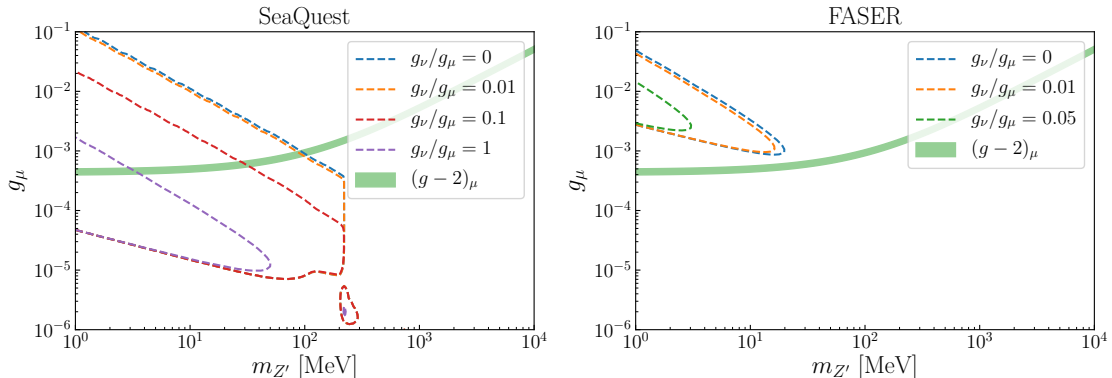


Figure 3.3. Similar to the right panel of Fig. 3.2, this time for SeaQuest (left) and FASER (right).

Table 1. Configurations of future BD experiments

Experiments	L_{sh} [meter]	L_{dec} [meter]	proton beam energy	Ref.
SHiP	60	50	400 GeV	[39]
SeaQuest	5	1	120 GeV	[23]
FASER	480	5×3	7 TeV	[28]

Eq. (2.12), which gives $g_p = -g_e$. Modifying this by an $\mathcal{O}(1)$ amount will not qualitatively change our conclusions.

As is shown in Fig. 3.2, the value of g_ν significantly affects the SHiP sensitivity to Z' . For $g_\nu = 0$, since there is no invisible decay, the Z' can only decay to electrons when $m_{Z'}$ is below 212 MeV. When it is above 212 MeV, the decay mode $Z' \rightarrow \mu\bar{\mu}$ opens and, due to the large coupling, the Z' lifetime drastically decreases, leading to a very substantial drop in the upper and lower bounds on g_μ . For $g_\nu = 0.2g_\mu$, the high-mass regime (> 212 MeV) is not significantly affected because $Z' \rightarrow \mu\bar{\mu}$ is still the dominant decay mode. In the low-mass regime, however, the branching ratio of invisible decay is enhanced, leading to a reduction of the upper bound by an order of magnitude. When g_ν further increases, both high- and low-mass regimes are affected. In particular, when $g_\nu/g_\mu = 2$, the sensitivity region is divided into two separate regions: $m_{Z'} \lesssim 80$ MeV and $m_{Z'} \gtrsim 212$ MeV.

The above analysis can be straightforwardly adapted to other similar BD experiments such as FASER and SeaQuest. We summarize their configurations in Tab. 1 and perform similar analyses. For SeaQuest, we adopt the result in Fig. 2 of Ref. [23] to determine the mass dependence of the production rate. The FASER experiment is based on 7+7 TeV proton collision at the LHC, and thus technically not a BD experiment. Nevertheless, we can treat it as a BD experiment because it is sensitive to Z' masses below 3 GeV, where proton bremsstrahlung and meson decays are the dominant processes for Z' production. Using Eq. (3.15), we successfully reproduce the anticipated dark photon results in both Ref. [23] (SeaQuest) and Ref. [28] (FASER). Like the above analysis for SHiP, we also find that the dependence of the results on $p_{Z'}$ is weak and the best fit is obtained when $p_{Z'}$ is

set at half the proton beam energy.

In Fig. 3.3, we recast the published dark photon bounds of SeaQuest and FASER to the bounds on Z' . For SeaQuest, we present the sensitivity reach of its Phase-I run with 1.44×10^{18} protons on target (POT). The result could be further improved by its Phase-II run with 10^{20} POT. Due to the uncertainty of the experimental configuration for its Phase II, we only include Phase I of SeaQuest in our analysis. For FASER, there are also two proposed configurations, with the integrated luminosity $\int dL$ and the decay volume L_{dec} given by $(\int dL, L_{\text{dec}}) = (150 \text{ fb}^{-1}, 1.5 \times 3 \text{ m})$ and $(3 \text{ ab}^{-1}, 5 \times 3 \text{ m})$ —see Sec. II E in [28]. We adopt the latter and find that even with the enhanced integrated luminosity, the FASER sensitivity still cannot reach the green $(g-2)_\mu$ band in Fig. 3.3. This is mainly due to the low collision rate of collider-based experiments compared to fixed-target experiments (3 ab^{-1} only corresponds to 2.3×10^{17} POT).

4 Combined results and discussions

Using the results obtained in the previous sections, in Fig. 4.1 we present the prospects of probing the Z' as a solution to the muon $g-2$ anomaly in future BD experiments. We show SHiP and SeaQuest sensitivity curves for $g_\nu/g_\mu = 1, 0.1, 0.01,$ and 0.001 . FASER results are absent due to their weak sensitivity—see the discussion in Sec. 3. Existing limits including BaBar- 4μ , Borexino, CCFR, and BBN&CMB are presented as solid black curves and their details have been explained in Sec. 2.3.

As we have discussed, the neutrino coupling g_ν plays a crucial role here because the invisible decay width can substantially weaken the sensitivity of BD experiments. On the other hand, a sizeable g_ν can be constrained by various neutrino scattering experiments. When g_ν increases, neutrino scattering bounds are stronger. When g_ν decreases, BD experiments provide more restrictive bounds. Therefore, constraints from BD and neutrino experiments are complementary to each other.¹¹

To show this complementarity, we adapt results from previous studies on neutrino trident scattering¹² (similar to CCFR) at the DUNE near detector [35] and coherent elastic neutrino-nucleus scattering (CE ν NS) at future COHERENT detectors [33]. The DUNE curves presented in Fig. 4.1 assume a 75 tonne LAr near detector with 5-year data taking for each of ν and $\bar{\nu}$ modes, and a 5% normalization uncertainty. The COHERENT curves assume 10 tonne-year exposure of NaI and Ar detectors with the current neutrino flux from the Spallation Neutron Source. When g_ν/g_μ varies, the neutrino scattering bounds are rescaled by a factor of $\sqrt{g_\nu/g_\mu}$.

As is shown in Fig. 4.1, for $g_\nu/g_\mu = 1$, future neutrino scattering experiments such as DUNE or COHERENT will be fully able to probe or exclude the Z' solution to muon $g-2$. Reducing g_ν can significantly alleviate neutrino scattering bounds but in this case

¹¹In this paper, we took $g_\nu = g_{\nu_\mu}$, and therefore $g_{\nu_e} = g_{\nu_\tau} = 0$, in order to directly compare bounds from BDs with those from muon neutrino scattering experiments. Introducing non-zero g_{ν_e} and g_{ν_τ} would modify this, however it would introduce a range of additional bounds e.g. the stringnet bound on electron neutrino scattering from TEXONO [49].

¹²Although ν - e elastic scattering at the DUNE near detector can also be sensitive to the Z' , in the low-mass limit it is about a factor of two weaker in terms of g_μ than the trident scattering.

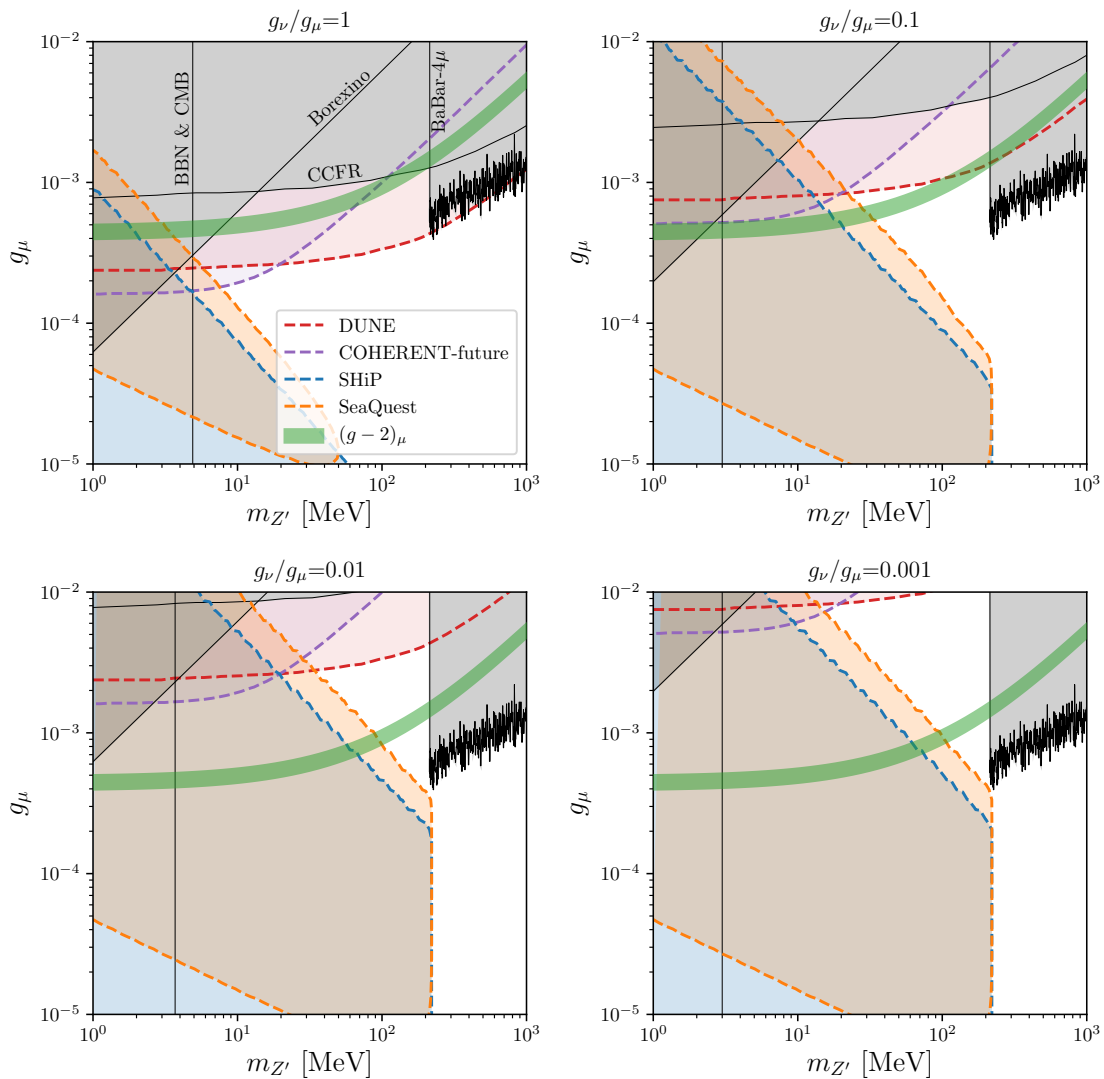


Figure 4.1. Prospects of future BD and neutrino experiments probing the Z' solution to the muon $g-2$ anomaly. The upper left panel assumes $g_\nu/g_\mu = 1$ and states the different bounds in the figure, the other panels with $g_\nu/g_\mu = 0.1, 0.01,$ and 0.001 employ the same conventions. Couplings of Z' to the electron and quarks are assumed to be at the loop-induced level given by Eq. (2.12).

SHiP and SeaQuest will provide rather restrictive constraints. For g_ν/g_μ varying from 1 to 0.001, the combination of future neutrino and BD experiments can generally probe most of the current viable parameter space of the Z' solution to the muon $g-2$ anomaly.

5 Conclusions

A light Z' is a simple and popular explanation for the muon $g-2$ anomaly. Within this class of solutions, in order to evade stringent experimental bounds, the Z' couplings to electrons and quarks have to be suppressed. In this work, we impose general lower bounds on these suppressed couplings by taking into account possible loop corrections, and study

the prospect of probing such a Z' in future BD experiments. After introducing the formalism and current experimental status in Sec. 2, we investigate in detail the sensitivity of future beam dump experiments in Sec. 3. When the Z' coupling to neutrinos is suppressed with respect to its coupling to muons, these beam dumps will have the capacity to rule out—or discover—a large portion of the successful Z' parameter space, despite the smallness of its coupling to electrons and quarks. For $g_\nu/g_\mu \lesssim 0.01$, SHiP and SeaQuest will rule out Z' explanations of the anomaly with $m_{Z'} \lesssim 100$ MeV, leaving only a fairly narrow window given that $m_{Z'} \gtrsim 2m_\mu$ is already excluded by BaBar 4μ . Models with larger Z' couplings to neutrinos somewhat circumvent these bounds, but are constrained by current or future neutrino scattering experiments. There is thus a powerful complementarity between beam dump and neutrino scattering experiments, as outlined in Sec. 4 and displayed in Fig. 4.1. The $g_\nu = g_\mu$ case, which arises for instance in the $L_\mu - L_\tau$ model, will be completely covered by the experiments we considered.

The muon $g - 2$ anomaly is particularly interesting not just because it is an indication of new physics, but because the nature of the anomaly suggests that the new physics, if it exists, may very well be discovered in the near future. This works highlights some promising avenues for such a potential discovery.

Acknowledgments

This work is supported by IISN convention No. 4.4503.15, by the “Probing dark matter with neutrinos” ULB-ARC convention, and by the F.R.S./FNRS under the Excellence of Science (EoS) project No. 30820817 - be.h “The H boson gateway to physics beyond the Standard Model”. R.C. thanks the UNSW School of Physics, where he is a Visiting Fellow, for their hospitality during this project.

References

- [1] **Muon g-2 Collaboration**, G. W. Bennett *et al.*, *Final Report of the Muon E821 Anomalous Magnetic Moment Measurement at BNL*, Phys. Rev. D **73** (2006) 072003, [[hep-ex/0602035](#)].
- [2] **Muon g-2 Collaboration**, B. Abi *et al.*, *Measurement of the Positive Muon Anomalous Magnetic Moment to 0.46 ppm*, Phys. Rev. Lett. **126** (2021), no. 14 141801, [[2104.03281](#)].
- [3] T. Aoyama *et al.*, *The anomalous magnetic moment of the muon in the Standard Model*, Phys. Rept. **887** (2020) 1–166, [[2006.04822](#)].
- [4] S. Borsanyi *et al.*, *Leading hadronic contribution to the muon magnetic moment from lattice QCD*, Nature **593** (2021), no. 7857 51–55, [[2002.12347](#)].
- [5] M. Pospelov, *Secluded $U(1)$ below the weak scale*, Phys. Rev. D **80** (2009) 095002, [[0811.1030](#)].
- [6] B. Holdom, *Two $U(1)$'s and Epsilon Charge Shifts*, Phys. Lett. B **166** (1986) 196–198.
- [7] P. Ilten, Y. Soreq, M. Williams, and W. Xue, *Serendipity in dark photon searches*, JHEP **06** (2018) 004, [[1801.04847](#)].

- [8] M. Bauer, P. Foldenauer, and J. Jaeckel, *Hunting All the Hidden Photons*, JHEP **18** (2020) 094, [[1803.05466](#)].
- [9] X. G. He, G. C. Joshi, H. Lew, and R. R. Volkas, *NEW Z-prime PHENOMENOLOGY*, Phys. Rev. **D43** (1991) 22–24.
- [10] R. Foot, *New Physics From Electric Charge Quantization?*, Mod. Phys. Lett. **A6** (1991) 527–530.
- [11] X.-G. He, G. C. Joshi, H. Lew, and R. R. Volkas, *Simplest Z-prime model*, Phys. Rev. **D44** (1991) 2118–2132.
- [12] W. Altmannshofer, S. Gori, M. Pospelov, and I. Yavin, *Neutrino Trident Production: A Powerful Probe of New Physics with Neutrino Beams*, Phys. Rev. Lett. **113** (2014) 091801, [[1406.2332](#)].
- [13] W. Altmannshofer, C.-Y. Chen, P. S. Bhupal Dev, and A. Soni, *Lepton flavor violating Z' explanation of the muon anomalous magnetic moment*, Phys. Lett. B **762** (2016) 389–398, [[1607.06832](#)].
- [14] M. Escudero, D. Hooper, G. Krnjaic, and M. Pierre, *Cosmology with A Very Light $L_\mu - L_\tau$ Gauge Boson*, JHEP **03** (2019) 071, [[1901.02010](#)].
- [15] R. Garani and J. Heeck, *Dark matter interactions with muons in neutron stars*, Phys. Rev. D **100** (2019), no. 3 035039, [[1906.10145](#)].
- [16] A. Bodas, R. Coy, and S. J. D. King, *Solving the electron and muon $g - 2$ anomalies in Z' models*, [2102.07781](#).
- [17] **BaBar Collaboration**, J. P. Lees et al., *Search for a muonic dark force at BABAR*, Phys. Rev. D **94** (2016), no. 1 011102, [[1606.03501](#)].
- [18] S. Andreas, C. Niebuhr, and A. Ringwald, *New Limits on Hidden Photons from Past Electron Beam Dumps*, Phys. Rev. D **86** (2012) 095019, [[1209.6083](#)].
- [19] **NA64 Collaboration**, D. Banerjee et al., *Improved limits on a hypothetical $X(16.7)$ boson and a dark photon decaying into e^+e^- pairs*, Phys. Rev. D **101** (2020), no. 7 071101, [[1912.11389](#)].
- [20] S. Alekhin et al., *A facility to Search for Hidden Particles at the CERN SPS: the SHiP physics case*, Rept. Prog. Phys. **79** (2016), no. 12 124201, [[1504.04855](#)].
- [21] **SHiP Collaboration**, M. Anelli et al., *A facility to Search for Hidden Particles (SHiP) at the CERN SPS*, [1504.04956](#).
- [22] S. Gardner, R. J. Holt, and A. S. Tadepalli, *New Prospects in Fixed Target Searches for Dark Forces with the SeaQuest Experiment at Fermilab*, Phys. Rev. D **93** (2016), no. 11 115015, [[1509.00050](#)].
- [23] A. Berlin, S. Gori, P. Schuster, and N. Toro, *Dark Sectors at the Fermilab SeaQuest Experiment*, Phys. Rev. D **98** (2018), no. 3 035011, [[1804.00661](#)].
- [24] Y.-D. Tsai, P. deNiverville, and M. X. Liu, *Dark Photon and Muon $g - 2$ Inspired Inelastic Dark Matter Models at the High-Energy Intensity Frontier*, Phys. Rev. Lett. **126** (2021), no. 18 181801, [[1908.07525](#)].
- [25] J. P. Chou, D. Curtin, and H. J. Lubatti, *New Detectors to Explore the Lifetime Frontier*, Phys. Lett. B **767** (2017) 29–36, [[1606.06298](#)].

- [26] J. A. Evans, *Detecting Hidden Particles with MATHUSLA*, Phys. Rev. D **97** (2018), no. 5 055046, [[1708.08503](#)].
- [27] J. L. Feng, I. Galon, F. Kling, and S. Trojanowski, *ForwArd Search ExpeRiment at the LHC*, Phys. Rev. D **97** (2018), no. 3 035001, [[1708.09389](#)].
- [28] **FASEr Collaboration**, A. Ariga et al., *FASEr’s physics reach for long-lived particles*, Phys. Rev. D **99** (2019), no. 9 095011, [[1811.12522](#)].
- [29] **FASEr Collaboration**, H. Abreu et al., *Detecting and Studying High-Energy Collider Neutrinos with FASEr at the LHC*, Eur. Phys. J. C **80** (2020), no. 1 61, [[1908.02310](#)].
- [30] V. V. Gligorov, S. Knapen, M. Papucci, and D. J. Robinson, *Searching for Long-lived Particles: A Compact Detector for Exotics at LHCb*, Phys. Rev. D **97** (2018), no. 1 015023, [[1708.09395](#)].
- [31] S. Bilmis, I. Turan, T. Aliev, M. Deniz, L. Singh, and H. Wong, *Constraints on Dark Photon from Neutrino-Electron Scattering Experiments*, Phys. Rev. D **92** (2015), no. 3 033009, [[1502.07763](#)].
- [32] M. Lindner, F. S. Queiroz, W. Rodejohann, and X.-J. Xu, *Neutrino-electron scattering: general constraints on Z' and dark photon models*, JHEP **05** (2018) 098, [[1803.00060](#)].
- [33] M. Abdullah, J. B. Dent, B. Dutta, G. L. Kane, S. Liao, and L. E. Strigari, *Coherent elastic neutrino nucleus scattering as a probe of a Z' through kinetic and mass mixing effects*, Phys. Rev. D **98** (2018), no. 1 015005, [[1803.01224](#)].
- [34] J. M. Link and X.-J. Xu, *Searching for BSM neutrino interactions in dark matter detectors*, JHEP **08** (2019) 004, [[1903.09891](#)].
- [35] P. Ballett, M. Hostert, S. Pascoli, Y. F. Perez-Gonzalez, Z. Tabrizi, and R. Zukanovich Funchal, *Z' s in neutrino scattering at DUNE*, Phys. Rev. D **100** (2019), no. 5 055012, [[1902.08579](#)].
- [36] P. S. B. Dev, D. Kim, K. Sinha, and Y. Zhang, *New Interference Effects from Light Gauge Bosons in Neutrino-Electron Scattering*, [2105.09309](#).
- [37] G. Chauhan and X.-J. Xu, *How dark is the ν_R -philic dark photon?*, JHEP **04** (2021) 003, [[2012.09980](#)].
- [38] X. Luo, W. Rodejohann, and X.-J. Xu, *Dirac neutrinos and N_{eff} . Part II. The freeze-in case*, JCAP **03** (2021) 082, [[2011.13059](#)].
- [39] **SHiP Collaboration**, C. Ahdida et al., *Sensitivity of the SHiP experiment to dark photons decaying to a pair of charged particles*, Eur. Phys. J. C **81** (2021), no. 5 451, [[2011.05115](#)].
- [40] G. 't Hooft, *Naturalness, chiral symmetry, and spontaneous chiral symmetry breaking*, NATO Sci. Ser. B **59** (1980) 135–157.
- [41] T. Araki, S. Hoshino, T. Ota, J. Sato, and T. Shimomura, *Detecting the $L_\mu - L_\tau$ gauge boson at Belle II*, Phys. Rev. D **95** (2017), no. 5 055006, [[1702.01497](#)].
- [42] P. S. B. Dev, W. Rodejohann, X.-J. Xu, and Y. Zhang, *MUonE sensitivity to new physics explanations of the muon anomalous magnetic moment*, JHEP **05** (2020) 053, [[2002.04822](#)].
- [43] J. P. Leveille, *The Second Order Weak Correction to $(G-2)$ of the Muon in Arbitrary Gauge Models*, Nucl. Phys. B **137** (1978) 63–76.

- [44] **CMS Collaboration**, A. M. Sirunyan *et al.*, *Search for an $L_\mu - L_\tau$ gauge boson using $Z \rightarrow 4\mu$ events in proton-proton collisions at $\sqrt{s} = 13$ TeV*, Phys. Lett. B **792** (2019) 345–368, [[1808.03684](#)].
- [45] **Borexino Collaboration**, G. Bellini *et al.*, *Precision measurement of the ${}^7\text{Be}$ solar neutrino interaction rate in Borexino*, Phys. Rev. Lett. **107** (2011) 141302, [[1104.1816](#)].
- [46] N. Sabti, J. Alvey, M. Escudero, M. Fairbairn, and D. Blas, *Refined Bounds on MeV-scale Thermal Dark Sectors from BBN and the CMB*, JCAP **01** (2020) 004, [[1910.01649](#)].
- [47] H. K. Dreiner, J.-F. Fortin, J. Isern, and L. Ubaldi, *White Dwarfs constrain Dark Forces*, Phys. Rev. D **88** (2013) 043517, [[1303.7232](#)].
- [48] **Particle Data Group Collaboration**, P. A. Zyla *et al.*, *Review of Particle Physics*, PTEP **2020** (2020), no. 8 083C01.
- [49] **TEXONO Collaboration**, M. Deniz *et al.*, *Measurement of $\text{Nu}(e)\text{-bar}$ -Electron Scattering Cross-Section with a CsI(Tl) Scintillating Crystal Array at the Kuo-Sheng Nuclear Power Reactor*, Phys. Rev. **D81** (2010) 072001, [[0911.1597](#)].